*sustainability*

MDPI

*Article*

# Assessment of the Impact of Climate Change on the Ecological Resilience of the Yangtze River Economic Belt

**Jianglin Yao [1], Hongliang Wu [1,2] and Feng Yan [1,*]**

[1] School of Infrastructure Engineering, Nanchang University, Nanchang 330031, China; bjtwdxszdy@163.com (J.Y.)
[2] PowerChina Guiyang Engineering Corporation Limited, Guiyang 550081, China
* Correspondence: yfmilan@163.com

**Abstract**

With climate change and frequent extreme weather events, ecological stability is facing threats. This study constructs a quantitative assessment model coupling climate change and ecological resilience (ER), explores the impact of future climate change on ER, and identifies key meteorological risks that affect ER. Taking the Yangtze River Economic Belt (YREB) as the research area, the main research results are as follows: (1) Under the four future scenarios, the Climate Change Impact Index (CCI) values for ER are −0.8005, −0.8924, −0.9540, and −1.2298, respectively, indicating a general decline in ER across the YREB. (2) The extent of climate change impacts varies significantly among scenarios, with the ranking SSP5-8.5 > SSP4-6.0 > SSP2-4.5 > SSP1-2.6. The SSP5-8.5 scenario exhibits the most severe impacts, with CCI values of −0.7015, −1.2910, −1.3124, and −1.6144. (3) Spatially, climate change exerts the greatest impact on the upstream regions, followed by the downstream and midstream areas. Among these, very high resilience and very low resilience levels experience the most pronounced changes. (4) Temperature (Temp) and the Normalized Difference Vegetation Index (NDVI) are the main meteorological risks for the deterioration of ER. In future scenarios, Temp demonstrates an increasing trend while NDVI shows a significant decline.

**Keywords:** climate change; ecological resilience; Yangtze River Economic Belt; quantitative impact assessment

check for updates

Academic Editors: Cheng Li, Fei Zhang, Mou Leong Tan and Kwok Pan Chun

Received: 14 June 2025
Revised: 19 July 2025
Accepted: 28 August 2025
Published: 15 September 2025

**Citation:** Yao, J.; Wu, H.; Yan, F. Assessment of the Impact of Climate Change on the Ecological Resilience of the Yangtze River Economic Belt. *Sustainability* **2025**, *17*, 8265. https://doi.org/10.3390/su17188265

**Copyright:** © 2025 by the authors. Licensee MDPI, Basel, Switzerland. This article is an open access article distributed under the terms and conditions of the Creative Commons Attribution (CC BY) license (https://creativecommons.org/licenses/by/4.0/).

## 1. Introduction

In 2023, the United Nations Intergovernmental Panel on Climate Change released its sixth assessment report, Climate Change 2023. This report notes that all regions around the world are facing unprecedented climate change, with increasingly frequent extreme heat, heavy rainfall, and regional droughts [1]. The increase in extreme weather events poses a threat to the sustainable development of the ecological environment. Multiple studies indicate that major river basins in China are facing impacts of climate change. Xue et al. predict an overall increasing trend of drought risk in Southwestern China based on CMIP6 model projections [2]. Wang et al. focus on the drought characteristics of the Han River Basin under future climate change scenarios [3]. Li et al. analyze the impacts of climate change on extreme hydrological events in the Wei River Basin and their solutions [4]. Liu et al.'s study on the Yellow River Basin under future climate scenarios shows significant increases in both temperature and precipitation across the basin [5].

The YREB spans Eastern, Central, and Western China and serves dual functions as both an economic growth engine and an ecological security barrier. However, the region has long been confronted with the contradiction between human development and nature, as well as between economic growth and ecological conservation, a situation further exacerbated by climate change. Li et al. argue that the ecological security of the Yangtze River Basin is impacted by climate change [6]. Hu et al. investigate the spatiotemporal evolution trends of meteorological drought in the Yangtze River Basin [7]. Wen et al. project significant increases in annual mean temperature and precipitation across the Yangtze River Basin based on N-CMIP6 simulations [8]. Local ecological restoration efforts have not yet fully achieved harmonious coexistence between humans and nature. Consequently, against the backdrop of current climate change-induced crises and challenges, how to address various risks and enhance emergency response capabilities has become one of the key issues for sustainable development in the YREB.

"Resilience" was originally a concept in physics, and later as a research paradigm with evolutionary dynamics and nonlinearity, it has received widespread attention from scholars in fields such as economics, society, and the environment. Ecologist Holling introduced the concept of resilience into ecology and gradually expanded it from natural ecology to human ecology [9]. The core concept of ER is how a system can maintain its stability as much as possible under external interference [10]. Currently, the ER of the YREB is showing a deteriorating trend, which also reflects the increasing conflict between its economic development and the ecological environment. At present, how to deal with various risks and maintain ER in the face of environmental pollution, resource scarcity, and ecosystem degradation caused by global climate change has become one of the important issues for regional sustainable development.

Climate change poses challenges to regional sustainable development, particularly as its impacts on urban vulnerability during urbanization processes should not be underestimated [11]. Cui et al.'s study reveals that climate change has persistent impacts on regional system operations, human settlement quality, and residents' lives and property security [12]. Terry Cannon & Detlef Müller-Mahn theoretically elaborate the conceptual development of vulnerability and resilience in the context of climate change [13]. Emma L. Tompkins & W. Neil Adger demonstrate through case studies that mechanisms for enhancing social–ecological resilience are typically embedded within communities and co-management institutions that respond to environmental changes, providing viable pathways for building climate-threat resilience [14]. Kim et al. assess urban resilience in South Korea by taking into account climate change impacts and classify the 232 cities nationwide [15]. Scholars worldwide have increasingly recognized that climate change is an indispensable factor in resilience research.

Currently, scholars both domestically and internationally have proposed multiple methods to quantify resilience. Lu et al. calculated resilience levels by combining Particle Swarm Optimization algorithms and Backpropagation Neural Networks, while using kernel density estimation to analyze the dynamic evolution process of urban agglomeration resilience [16]. Tang et al. established an urban resilience evaluation index system using system dynamics methodology and simulated the changes in urban resilience in the YREB [17]. Xia et al. evaluated urban resilience in the Yangtze River Delta from 2010 to 2020 using the TOPSIS method, Particle Swarm Optimization, and Extreme Learning Machine approaches [18]. Liu et al. applied the panel vector autoregression model to quantify climate change impacts on resilience variations in the Beijing–Tianjin–Hebei region from 1998 to 2019 [19].

To date, existing research on ER remains limited. Existing studies primarily analyze climate change and ER as separate subjects, and even those that integrate both topics show

limited research depth. Furthermore, although there are currently methods for quantifying resilience, most of them are complex and lack models that quantitatively assess the impact of climate change on ER. As a crucial ecological barrier and economic development zone in China, the YREB has seen increased research on ER, but these limitations persist.

To address the dual limitations of insufficient integration between climate change and ER research and the lack of quantitative models to assess climate change impacts on resilience, this study develops a coupled quantitative assessment model that integrates climate change and ER based on CMIP6 model data, using the YREB as a case study to investigate future climate change impacts on ER. The innovations of this work are twofold: (1) establishing a climate–ER coupling model to quantify climate change effects on ER dynamics; and (2) identifying key climatic risk factors affecting ER. This study provides a scientific foundation for the formulation of regional ecological protection policies and holds significant implications for sustainable development and climate-adaptive management of the YREB.

## 2. Methods and Materials

### *2.1. Study Area*

The YREB is an important economic region in China, spanning across the three major regions of East, West, and Central China, covering the Yangtze River and its basin, and playing an important role in China's economic development. The YREB covers 11 provinces and municipalities, including Shanghai, Jiangsu, Zhejiang, Anhui, Jiangxi, Hubei, Hunan, Chongqing, Sichuan, Guizhou, and Yunnan (Figure 1), with an area of approximately 2,052,300 km$^2$, accounting for 21.40% of the country's total. This region is one of the most important agricultural, industrial, and transportation hubs in China, with abundant resources and a significant population base, accounting for over 40% of the country's total economic output and population [20]. As a key area for biodiversity conservation in China, the YREB plays a crucial role in maintaining soil conservation and biodiversity [21].

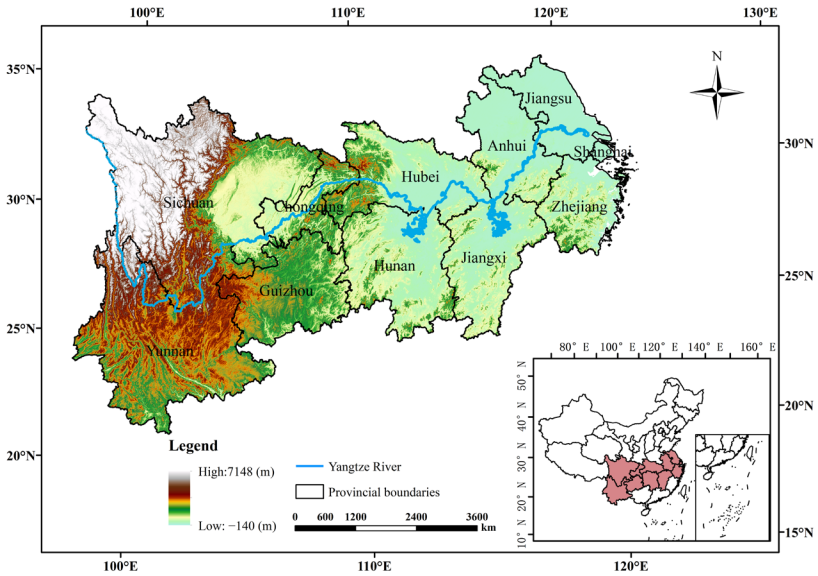


**Figure 1.** A schematic diagram of the Yangtze River Economic Belt region.

However, in the context of climate change, the YREB is facing many challenges and pressures. The increase in precipitation and temperature caused by climate change has a critical impact on its ecosystem and water resource management. The YREB is facing a series of problems such as reduced forest coverage, ecological degradation, water loss, and shortage of water resources.

### *2.2. Data Sources*

#### 2.2.1. Climate Data

The temperature and precipitation observation data were obtained from the China Surface Temperature and Precipitation Monthly 0.5° × 0.5° Gridded Dataset (V2.0) released by the National Meteorological Information Center. The CMIP6 global climate model data were downloaded from the ESGF platform, including historical simulation data (1985–2014) of monthly temperature and precipitation. The future scenario data (2021–2100) was under four Shared Socioeconomic Pathways: SSP1-2.6 (sustainable development with low radiative forcing), SSP2-4.5 (intermediate development with medium radiative forcing), SSP4-6.0 (uneven development with medium radiative forcing), and SSP5-8.5 (fossil-fueled development with high radiative forcing). Three climate models were selected for this study (Table 1), and all model data were uniformly downscaled to a 10 km × 10 km spatial resolution using bilinear interpolation.

**Table 1.** Basic information of three CMIP6 climate models.

| Model Name | Country | Atmospheric Resolution (Grid Points) |
|---|---|---|
| CanESM5 | Canada | 64 × 128 |
| MIROC6 | Japan | 128 × 256 |
| MRI-ESM2-0 | Japan | 160 × 320 |

#### 2.2.2. Remote Sensing and Geographical Data

The NDVI data for the YREB were acquired from the Resource and Environmental Science Data Platform, with a spatial resolution of 30 m × 30 m and temporal resolution of one year. Land use data were acquired from the Resource and Environmental Science Data Platform, with a spatial resolution of 30 m × 30 m. Digital Elevation Model (DEM) data were obtained from the Geospatial Data Cloud, with a spatial resolution of 30 m × 30 m. Using the resampling function in ArcGIS 10.2 software, all NDVI, land use, and DEM raster data were interpolated to a 10 km × 10 km grid.

#### 2.2.3. Socioeconomic Data

The socioeconomic data for the YREB were primarily collected from the China City Statistical Yearbook, China County (City) Socioeconomic Statistical Yearbook, and provincial statistical yearbooks and bulletins for corresponding years.

### *2.3. Methods*

#### 2.3.1. Construction of ER Evaluation Index System

Building a reasonable index system is crucial to accurately assess ER. Taking into account the impact of society, economy, and nature on ER, drawing on the existing literature's evaluation system for ER, and considering the availability of data, this study selects seven indicators, as shown in Table 2, to construct an evaluation system for ER in the YREB.

The Analytic Hierarchy Process (AHP) primarily considers human decision-making and exhibits strong subjectivity, potentially leading to arbitrariness during the weighting process. In contrast, the Entropy Weight Method (EWM) relies on objective data with stronger objectivity but fails to reflect the influence of human factors. Therefore, this study employs a combined EWM-AHP approach to determine the weights of each indicator. The specific formula can be found in reference [22,23]. The detailed weight calculation process is outlined in Appendix A.

**Table 2.** ER assessment system for YREB.

| Target Layer | Index Layer | The Nature of Indicators | EWM Weight | AHP Weight | Comprehensive Weight | Reference for Indicator Selection |
|---|---|---|---|---|---|---|
| ER | Normalized Difference Vegetation Index | + | 0.4612 | 0.5388 | 0.1783 | [24] |
| | Standardized Precipitation Evapotranspiration Index | − | 0.5163 | 0.4837 | 0.1027 | [25] |
| | Annual temperature (°C) | − | 0.4093 | 0.5907 | 0.2327 | |
| | Soil Sensitivity Index | − | 0.4102 | 0.5898 | 0.0629 | [26] |
| | The proportion of public financial expenditure (%) | + | 0.5969 | 0.4031 | 0.0260 | [27] |
| | Technology investment (billion) | + | 0.4039 | 0.5961 | 0.0612 | [28] |
| | Educational investment (billion) | + | 0.4946 | 0.5054 | 0.0335 | [28] |
| | Population density (persons/km$^2$) | − | 0.5372 | 0.4628 | 0.1310 | [29] |
| | Environmental protection expenditure (million dollars) | + | 0.6820 | 0.3180 | 0.0979 | [29] |
| | Proportion of foreign direct investment to GDP (%) | + | 0.7286 | 0.2714 | 0.0738 | [30] |

The NDVI serves as a critical index for assessing vegetation coverage and ecosystem health [24]. As the primary component of terrestrial ecosystems, vegetation dynamics directly reflect the resilience capacity of ecosystems and the quality of the ecological environment. The Standardized Precipitation Evapotranspiration Index (SPEI), which integrates the effects of precipitation and evapotranspiration, is widely recognized as a robust metric for evaluating drought and moisture conditions [25]. In the context of climate change, extreme precipitation and temperature are becoming increasingly frequent, and SPEI can effectively reflect the impact of these changes on ecosystems. Annual temperature is a key meteorological element that affects the stability of ecosystems. Climate change leads to an increase in temperature, which directly affects species distribution and the structure and function of ecosystems. The Soil Sensitivity Index (SSI) is selected as an evaluation index, as it effectively reflects ecosystem stability and the conservation status of land resources [26].

The proportion of public financial expenditure reflects the government's investment and management capacity in ecological environment protection, and social support is an important guarantee for ecosystem stability [27]. The increase in technology investment helps inject new momentum into economic development, thereby improving resource utilization and input/output ratio, while enhancing the ability to control ecological environment pollution and reducing corporate pollution emissions. The increase in education investment helps to enhance the comprehensive quality of workers and strengthen the recovery ability of economic and ecological systems after external disturbances [28]. Population density reflects the degree of population agglomeration, and both high and low population densities can have a negative impact on resilience, which is used as an evaluation indicator [29]. The ratio of foreign direct investment to GDP can not only reflect the degree of openness of a city to the outside world, but also indirectly reflect the stability of its economic operation. Foreign investment is more likely to flow into regions with stable markets and society [30]. Environmental protection expenditures reflect people's ability to protect and restore the ecological environment [29].

#### 2.3.2. Methods for Processing Meteorological Elements Under Climate Change

1. Downscaling method

This study uses precipitation and temperature data from three climate models, each with different resolutions. In order to eliminate differences in subsequent calculations, the model data is uniformly interpolated to the corresponding stations in the study area using a bilinear interpolation method [31]. The formula is as follows:

$$F = \left(\frac{x_2 - x_1}{x_2 - x}F_1 + \frac{x - x_1}{x_2 - x_1}F_2\right)\frac{y_2 - y}{y_2 - y_1} + \left(\frac{x_2 - x}{x_2 - x}F_3 + \frac{x - x_1}{x_2 - x}\right)F_4\frac{y - y_1}{y_2 - y_1} \quad (1)$$

where $x$ and $y$ represent the latitude and longitude of the location point, $x_1$ and $x_2$ represent the longitude of known points, and $y_1$ and $y_2$ represent the latitude of known points.

2. Deviation correction method

The varying degrees of deviation between the simulated results of a single mode and the measured values must be corrected. To reduce the limitations of the simulation, the linear scaling method is used to correct for bias in the downscaled results [32]. Finally, monthly data of 10 km × 10 km is obtained. The formula is as follows:

$$P_s(t) = P_m(t)(P_a/P_m) \quad (2)$$

$$T_s(t) = T_m(t) + (T_a - T_m) \quad (3)$$

where $t$ represents the year. $P_s(t)$ and $T_s(t)$ are the corrected monthly precipitation and temperature forecast data for the $t$-th year, respectively. $P_m(t)$ and $T_m(t)$ are the precipitation and temperature data of the climate model in the $t$-th year before calibration, respectively. $P_a$ and $T_a$ are the mean values of observed precipitation and temperature in the $m$-th month of the periodic period, while $P_m$ and $T_m$ are the mean values of predicted precipitation and temperature in the $m$-th month of the periodic period. The unit of precipitation data in the formula is mm, and the unit of temperature data is °C.

2.3.3. Soil and Water Loss Sensitivity Index

Soil erosion refers to the simultaneous loss of water and soil due to the influence of natural or human factors, the inability of rainwater to be absorbed in situ, downstream flow, and soil erosion [33]. The specific method for evaluating the soil and water loss sensitivity by hydrodynamics is as follows.

$R$ can be calculated by [34]

$$R = 0.0668P_d^{1.6266} \quad (4)$$

where $R$ is the annual average rainfall erosivity factor (MJ·mm/(hm$^2$·h)), and $P_d$ is the annual average rainfall.

$K$ can be calculated by [33]

$$K = \left\{0.2 + 0.3\exp\left[-0.0256S_a\left(1 - \frac{S_i}{100}\right)\right]\right\} \times \left[\frac{S_i}{C_l + S_i}\right]^{0.3} \times \left[1 - \frac{0.25\mathrm{OM}}{\mathrm{OM} + \exp(3.72 - 2.95\mathrm{OM})}\right] \times \left[1 - \frac{0.7SN_i}{SN_i + \exp(-5.51 + 22.9SN_i)}\right] \quad (5)$$

where $K$ is the soil erodibility factor ((t hm$^2$ h)/(hm$^2$·MJ·mm)). $S_a$, $S_i$, $C_l$, and OM refer to the proportion of sand (0.05~2 mm), silt (0.002~0.05 mm), clay particles (<0.002 mm), and organic matter in the American soil particle classification standard (%). $SN$ in the formula is calculated using $SN = 1 - S_a/100$.

The slope length and slope value $LS$ can be calculated by [34]

$$L = \left(\frac{\lambda}{22.13}\right)^m \tag{6}$$

$$\lambda = l \times \cos\alpha \tag{7}$$

where $L$ represents the slope length value, and $\lambda$ is the horizontal projection slope length (m). $l$ is the length of water flow along the surface flow direction, and $\alpha$ is the slope value of the water flow area. $m$ is a variable slope index, where m = 0.2, when $\theta < 0.57^\circ$, m = 0.3, when $0.57^\circ \leq \theta < 1.72^\circ$, m = 0.4, when $1.72^\circ \leq \theta < 2.86^\circ$, and m = 0.5, when $2.86^\circ \leq \theta$ [35].

The slope calculation is based on grading, with the McCool D K formula used for calculations below 10° and the Liu et al. formula used for calculations above 10° [34].

$$S = \begin{cases} 10.80 \times \sin\theta + 0.03 & \theta < 5^\circ \\ 16.80 \times \sin\theta - 0.50 & 5^\circ < \theta \leq 10^\circ \\ 21.91 \times \sin\theta - 0.96 & \theta > 10^\circ \end{cases} \tag{8}$$

$C$ can be calculated by [22]

$$\mathrm{FCV} = \frac{\mathrm{NDVI} - \mathrm{NDVI_{min}}}{\mathrm{NDVI_{max}} - \mathrm{NDVI_{min}}} \tag{9}$$

$$C = \begin{cases} 1 & \mathrm{FVC} \leq 0.095 \\ 0.6508 - 0.3436\mathrm{lgFVC} & 0.095 < \mathrm{FVC} < 0.783 \\ 0 & \mathrm{FVC} > 0.783 \end{cases} \tag{10}$$

where FCV stands for vegetation coverage, and NDVI is the Normalized Difference Vegetation Index.

$SSI_i$ can be calculated by

$$SSI_i = \sqrt[4]{R_i \times K_i \times LS_i \times C_i} \tag{11}$$

where $SSI_i$ represents the soil and water loss sensitivity index of the $i$-th spatial unit, and $R_i$ is the value for the annual average rainfall erosivity factor for the $i$-th unit space. $K_i$ represents the soil erodibility factor of the $i$-th spatial unit, $LS_i$ is the slope length and slope value of the $i$-th spatial unit, and $C_i$ is the vegetation cover management factor of the $i$-th spatial unit.

#### 2.3.4. Standardized Precipitation Evapotranspiration Index

SPEI comprehensively considers meteorological factors such as temperature, precipitation, humidity, and evapotranspiration, and can characterize extreme precipitation under the background of climate change at multiple spatiotemporal scales. The method for calculating SPEI is as follows [36].

The monthly potential evaporation $\mathrm{PET}_i$ can be calculated using the Thornthwaite method.

$$\mathrm{PET}_i = 16K\left(\frac{10t}{I}\right)^M \tag{12}$$

where $K$ is the correction coefficient calculated based on longitude and latitude, $t$ is the monthly average temperature, and $I$ is the annual total heating index. $M$ is the coefficient determined by $I$. $M = 0.00000675I^3 - 0.0000771I^2 + 0.01792I + 0.49$.

$D_i$ can be calculated by

$$D_i = p_i - \mathrm{PET}_i \tag{13}$$

where $D_i$ is the difference between monthly precipitation and potential evaporation, and $p_i$ represents monthly precipitation.

Log-Logistic is used to fit and normalize the data sequence. P and $\omega$ can be calculated by

$$\omega = \sqrt{-2\ln \mathrm{P}} \tag{14}$$

$$\mathrm{SPEI} = \begin{cases} \omega - \frac{c_0 + c_1\omega + c_2\omega^2}{1 + d_1\omega + d_2\omega^2 + d_3\omega^3} & (P \le 0.5) \\ -\left(\omega - \frac{c_0 + c_1\omega + c_2\omega^2}{1 + d_1\omega + d_2\omega^2 + d_3\omega^3}\right) & (P > 0.5) \end{cases} \tag{15}$$

where P is the probability of exceeding a certain $D_i$ value, and $\omega$ is the probability weighted distance. $c_0$ = 2.515517, $c_1$ = 0.802853, $c_2$ = 0.010380, $d_1$ = 0.432788, $d_2$ = 0.189269, $d_3$ = 0.001308.

#### 2.3.5. Normalized Difference Vegetation Index

The NDVI is an objective measure of changes in vegetation coverage and is the best indicator of vegetation growth and coverage. To predict the NDVI in the future, a regression model is constructed based on the impact of climate factors on vegetation growth, including precipitation and temperature [37]. $\mathrm{NDVI_i}$ can be calculated by

$$\mathrm{NDVI}_i = a_i \times P_i + T_i \times c_i \tag{16}$$

where NDVI is the historical scenario NDVI time series data. $P_i$ is the annual precipitation, and $T_i$ is the annual temperature. $a_i$, $b_i$, and $c_i$ are the regression coefficients for each spatial unit.

#### 2.3.6. Standardization of Indicators

In order to eliminate possible dimensional and magnitude differences between indicator data, this article adopts a range normalization method to standardize the original data [20].

Positive indicators can be calculated by

$$x'_{ij} = \frac{x_{ij} - \min(x_{1j}, x_{2j}, \ldots, x_{ij})}{\max(x_{1j}, x_{2j}, \ldots, x_{ij}) - \min(x_{1j}, x_{2j}, \ldots, x_{ij})} \tag{17}$$

Negative indicators can be calculated by

$$x'_{ij} = 1 - \frac{x_{ij} - \min(x_{1j}, x_{2j}, \ldots, x_{ij})}{\max(x_{1j}, x_{2j}, \ldots, x_{ij}) - \min(x_{ij}, x_{2j}, \ldots, x_{ij})} \tag{18}$$

where $x'_{ij}$ is the standardized value for the $i$-th spatial unit under the $j$-th indicator, and $x_{ij}$ represents the value of the $i$-th spatial unit under the $j$-th indicator before standardization. $\min(x_{1j}, x_{2j}, \ldots, x_{ij})$ is the minimum value of the $j$-th indicator throughout the entire study period, and $\max(x_{1j}, x_{2j}, \ldots, x_{ij})$ is the maximum value of the $j$-th indicator throughout the entire study period.

After standardization, the values of the resilience indicators were all between 0 and 1. Calculate the mean of each indicator in the target layer and criterion layer separately $\mu$, and standard deviation $\sigma$. According to the deviation method, the resilience level is divided into very low, low, moderate, high, and very high resilience levels. The classification of resilience levels is shown in Table 3.

**Table 3.** Resilience level classification.

| Resilience Level | Very Low Resilience | Low Resilience | Moderate Resilience | High Resilience | Very High Resilience |
|---|---|---|---|---|---|
| Temp | [0, 0.2) | [0.2, 0.4) | [0.4, 0.6) | [0.6, 0.8) | [0.8, 1.0] |
| NDVI | [0, 0.2) | [0.2, 0.4) | [0.4, 0.6) | [0.6, 0.8) | [0.8, 1.0] |
| SPEI | [0, 0.2) | [0.2, 0.4) | [0.4, 0.6) | [0.6, 0.8) | [0.8, 1.0] |
| SSI | [0, 0.2) | [0.2, 0.4) | [0.4, 0.6) | [0.6, 0.8) | [0.8, 1.0] |
| ER | [min, 0.43) | [0.43, 0.48) | [0.48, 0.53) | [0.53, 0.58) | [0.58, max] |
| Grade | 1 | 2 | 3 | 4 | 5 |

### *2.4. Evaluation Model for ER in Response to Climate Change*

To quantify the impact of climate change on ER, this study establishes a quantitative assessment model coupling climate change and ER based on CMIP6 model data. This model generates the CCI, which is used to quantify the magnitude and directional change in climate impacts on ER. Furthermore, the index enables the systematic identification of critical climatic risk drivers affecting ER. The specific calculation method is as follows.

The level change value $n_i$ of spatial units during the future period can be calculated by

$$n_i = \left| G_i' - G_i \right| \tag{19}$$

In the formula, $G_i'$ represents the level value corresponding to the $i$-th spatial unit value $x_i'$ in the future simulation period (Table 3), and $G_i$ represents the level value corresponding to the $i$-th spatial unit value $x_i$ in the historical experimental period. $n_i$ is the change value of the level of the $i$-th spatial unit in the future simulation period and historical experimental period.

The $\mathrm{CCI}_i$ for future simulation period spatial units can be calculated by

When $x_i' = x_i$, $\mathrm{CCI}_i = 0$.

When $x_i' > x_i$,

$$\mathrm{CCI}_i = \begin{cases} -\left(\frac{x_i' - D_i'}{x_i - D_i'}\right) + (n_i + 1) & (n_i = 0) \\ \frac{x_i' - D_i'}{\Delta} + (n_i + 1) & (n_i \neq 0) \end{cases} \tag{20}$$

When $x_i' < x_i$,

$$\mathrm{CCI}_i = \begin{cases} \frac{x_i' - D_i}{x_i - D_i} - (n_i + 1) & (n_i = 0) \\ \frac{x_i' - D_i}{\Delta} - (n_i + 1) & (n_i \neq 0) \end{cases} \tag{21}$$

$$\Delta = \left| D_{ij}' - D_{ij} \right| \tag{22}$$

In the formula, $x_i'$ is the $i$-th spatial unit value in the future simulation period, and $x_i$ is the $i$-th spatial unit value during the historical experimental period. $D_i$ is the upper limit of the interval that corresponds to level $x_i'$, and $D_i$ is the lower limit of the interval that corresponds to level $x_i'$. $\Delta$ is the absolute value of the difference between the upper and lower limits of the corresponding level interval for $x_i'$.

Based on the computed CCI values for each spatial unit, the regional-scale CCI was aggregated using the Zonal Statistics function in ArcGIS.

$$\mathrm{CCI} = \frac{\sum \mathrm{CCI}_i}{N} \tag{23}$$

where $\sum \mathrm{CCI}_i$ is the sum of the evaluation index for spatial units in various provinces and municipalities during the future simulation period. $N$ is the total number of spatial units in each region.

The CCI values indicate the following impacts of climate change:

1. CCI > 0: Signifies a positive impact of climate change.
2. CCI = 0: Denotes negligible climate change effects.
3. CCI < 0: Reflects a negative impact of climate change.

### *2.5. ER Evaluation Model Under Climate Change*

Typically, the process of establishing a quantitative assessment model for coupling climate change and ER can be described as a flowchart, as shown in Figure 2.

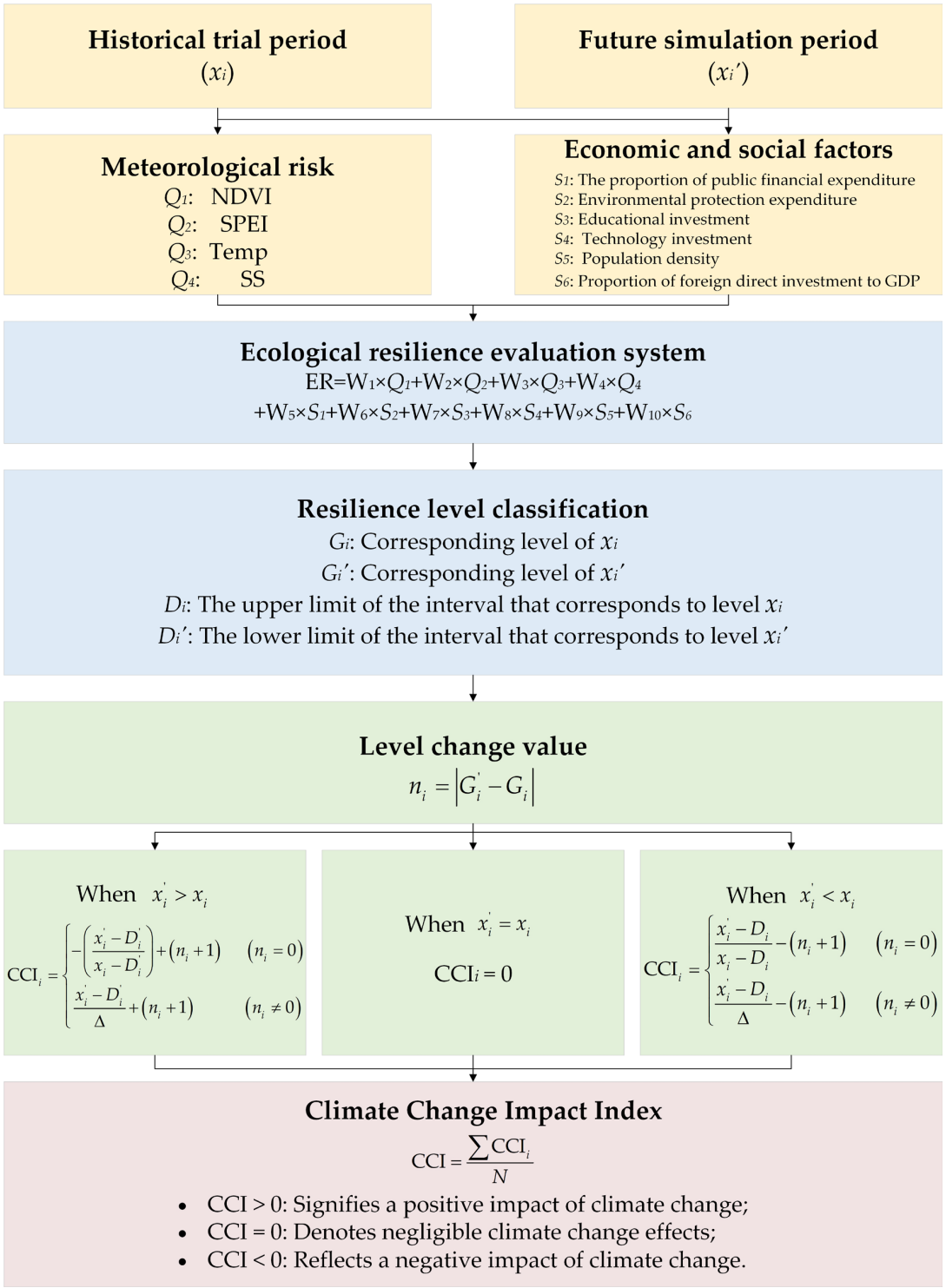


**Figure 2.** Procedures of ER evaluation model.

## 3. Results

### *3.1. Evaluation of Spatiotemporal Changes in Meteorological Risks*

The changes in NDVI, Temp, SPEI, and SSI due to climate change greatly affect ER. The normalized values of the indicators can to some extent reflect the changes in the indicators. Figure 3 presents the normalized mean values of the four indicators for the years 2030, 2060, 2075, and 2100 under the historical scenario and four different future scenarios.

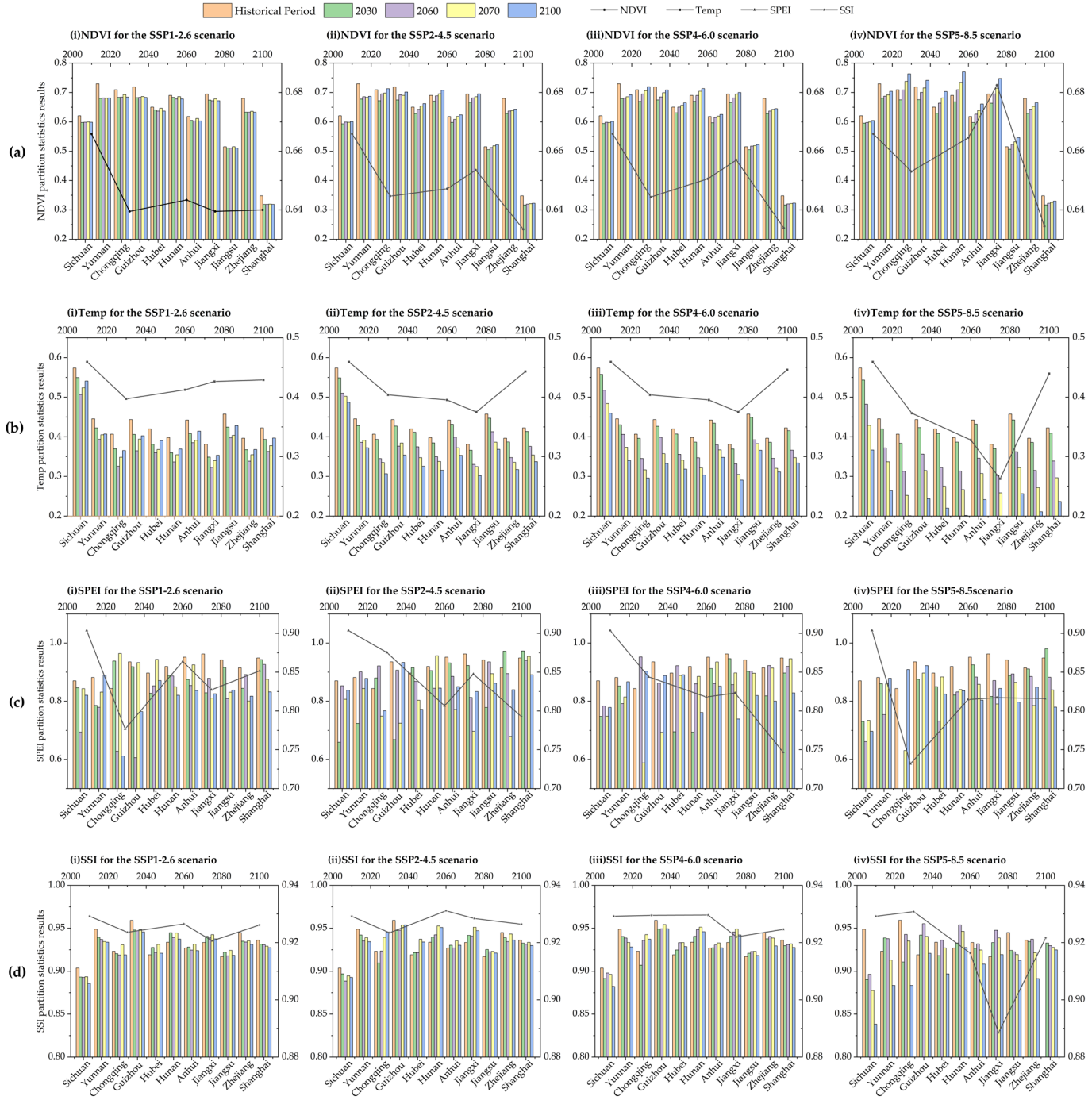


**Figure 3.** (**a**) The normalized mean values of NDVI; (**b**) the normalized mean values of Temp; (**c**) the normalized mean values of SPEI; (**d**) the normalized mean values of SSI.

Overall, compared to the historical scenario, NDVI (Figure 3a) and SPEI (Figure 3c) show a downward trend, while Temp (Figure 3b) shows an upward trend. Although the value of SSI (Figure 3d) has not changed much, it still decreases overall. Compared

to the changes in meteorological factors under the four future scenarios, the NDVI of the SSP1-2.6 scenario shows the most severe decrease, while the Temp of SSP4-6.0 and SSP5-8.5 considerably increase. In the SSP5-8.5 scenario, the decrease in SPEI and SSI is relatively noticeable. The future trends in Temp and SPEI in this study are consistent with the research of Sun on climate change in the Yangtze River Basin from 2006 to 2100 [35].

Among them, in terms of time, NDVI shows a prominent decline in the SSP1-2.6 scenario in 2060 and 2100, SSP2-4.5 in 2030, SSP4-6.0 in 2030, and SSP5-8.5 in 2030, with NDVI values of 0.6395, 0.6395, 0.6334, 0.6338, and 0.6344, respectively. Notably, SSP2-4.5 has the lowest NDVI value in 2030, at 0.6334. From a spatial perspective, the NDVI values in Sichuan, Hubei, Anhui, Jiangsu, and Shanghai are relatively low, with Shanghai having the lowest NDVI values in different future scenarios, ranging from 0.3168 to 0.3480. The trend of NDVI changes in this study is consistent with the research results of Fu et al. on the dynamic changes in vegetation in the Yangtze River Basin [1].

Although the temperature will increase in different scenarios in the future, it is most pronounced in the SSP4-6.0 and SSP5-8.5 scenarios. Due to Temp being a negative indicator, the smaller the normalized value, the more severe the Temp increases. The Temp values for the SSP4-6.0 scenario in 2075 and 2100 and for SSP5-8.5 scenario in 2060, 2070, and 2100 are 0.3794, 0.3566, 0.3729, 0.3280, and 0.2627, respectively. Clearly, the SSP5-8.5 scenario has the lowest Temp in 2100, reaching 0.2627. From a spatial distribution perspective, the high temperature situation is primarily located in the middle and lower reaches of the YREB, particularly in Hunan, Hubei, Jiangxi, and Zhejiang, with a temperature value between 0.1876 and 0.4423.

Although the numerical changes in SPEI and SSI are not as prominent as those in NDVI and Temp, they show a downward trend overall. The SPEI experienced a marked decrease in 2030 under the SSP4-6.0 scenario and 2060 under the SSP5-8.5 scenario, with SPEI values of 0.7469 and 0.7319, respectively. Chongqing and Guizhou, located in the upper reaches of the YREB, have the lowest SPEI values, ranging from 0.3251 to 0.9032. The SSI experienced the most severe decline in the SSP5-8.5 scenario in 2100, with a value of 0.8885. From a spatial perspective, the SSI values in Sichuan, Yunnan, and Chongqing in the upper reaches of the YREB are relatively low, ranging from 0.9483 to 0.9455. The SPEI change trend in Guizhou in this study is basically consistent with the results of Han et al. on extreme climate research in Guizhou from 2011 to 2050 [38].

### *3.2. Analysis of CCI Results for Meteorological Risks*

Based on the model proposed in Section 2.4, the CCI for four meteorological risks in 2030, 2060, 2075, and 2100 under four future scenarios were calculated. The resulting CCI values are presented as clustered bar charts in Figure 4.

According to Figure 4a, although the CCI of NDVI has both positive and negative values, overall NDVI shows a worsening trend with evaluation indices of −0.1744, −0.1207, −0.0964, and 0.0587, respectively. The deterioration trend of NDVI is particularly noticeable in the SSP1-2.6, SSP2-4.5, and SSP4-6.0 scenarios. The NDVI of Yunnan is most severely affected by climate change in four scenarios, with CCI values of −0.4941, −0.5238, −0.4667, and −0.4035, respectively. This implies that the vegetation coverage in Yunnan will decrease during the future simulation period, and the environmental degradation will be more severe. In 2075 and 2100, the CCI values of Chongqing, Hubei, Hunan, Jiangxi, Anhui, and Shanghai are positive, indicating an improvement in the NDVI situation in these areas. Among them, Hunan has the highest CCI in 2100, with values of −0.1086, 0.2312, 0.2952, and 0.8219, respectively. The trend of NDVI changes in Guizhou in this study is basically consistent with the predictions of Li et al. regarding vegetation covered under climate change from 2021 to 2100 [39].

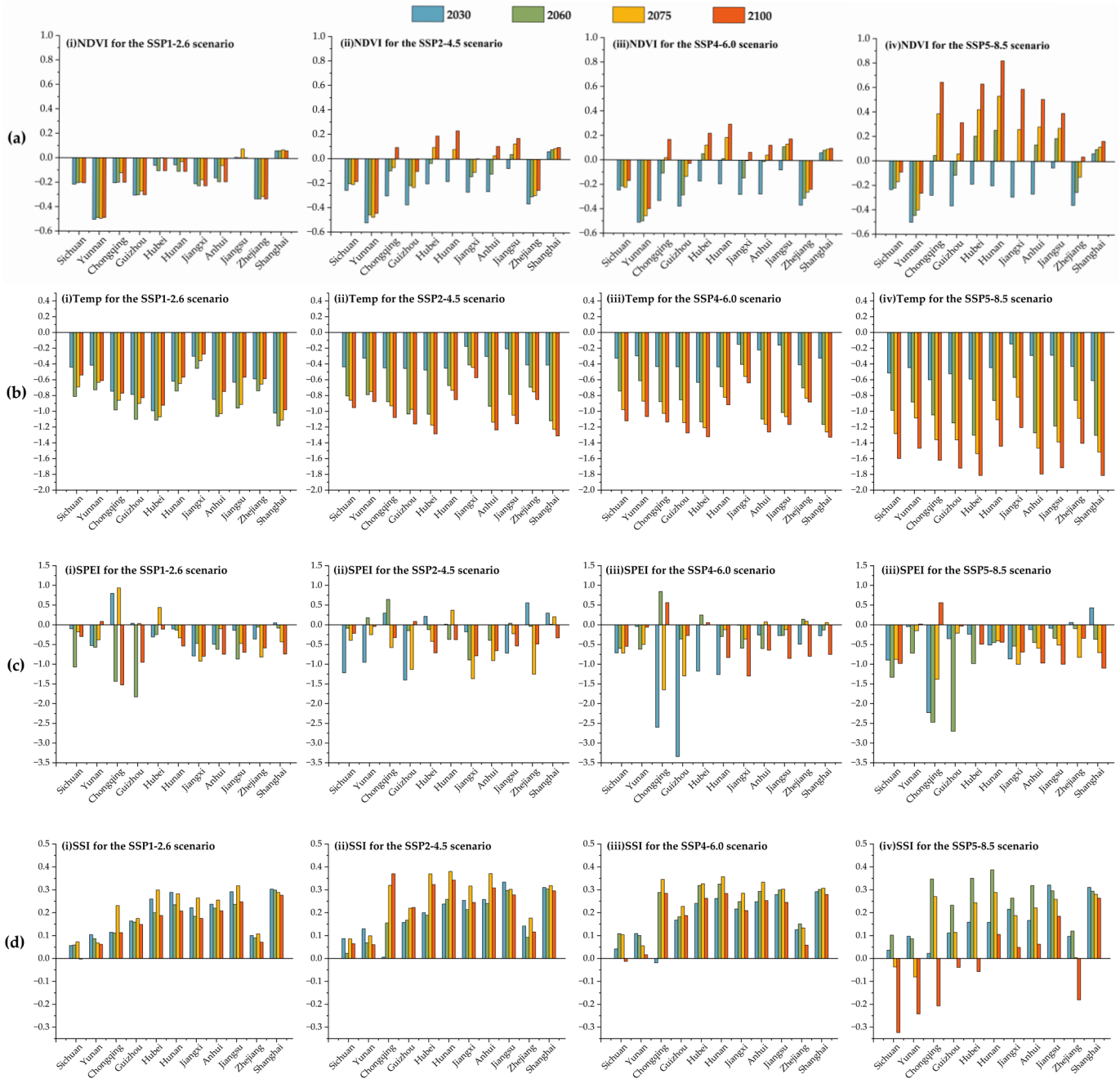


**Figure 4.** (**a**) CCI bar charts for NDVI; (**b**) CCI bar charts for Temp; (**c**) CCI bar charts for SPEI; (**d**) CCI bar charts for SSI.

It can be clearly seen that Temp is negative in all four scenarios (Figure 4b), with the CCI of −0.7630, −0.7884, −0.8229, and −1.0902, respectively. This indicates that Temp is a major meteorological risk affecting the ER of the YREB. High temperature has a deteriorating impact on ER. Notably, in Shanghai in 2100, the Temp is the most significant factor with CCI values of −0.9818, −1.3126, −1.3295, and −1.8154 for the four scenarios, respectively. Secondly, Hubei, Chongqing, Jiangsu, and Zhejiang are greatly affected by the Temp. However, Jiangxi is relatively less affected by Temp with CCI values of −0.3481, −0.4023, −0.4391, and −0.6862, respectively. The trend of temperature changes in this study is basically consistent with the research results of Wen et al. on temperature in the Yangtze River Basin from 2021 to 2100 [8].

The CCI of SPEI generally shows a decreasing trend during the future simulation period (Figure 4c). The decrease in the upper reaches of the YREB is greater than that

in the middle and lower reaches. Clearly, Guizhou has the lowest CCI for SSP4-6.0 in 2030, with a score of −3.3426. Additionally, there is also an improvement in the SPEI of Chongqing under four scenarios, particularly in the 2075 years of SSP1-2.6 scenario, with a CCI value of 0.9363. Overall, SSI shows improvement, with CCI values ranging from 0.0059 to 0.3872 (Figure 4d). However, the SSP5-8.5 of 2100 in the upper part of the YREB as well as Hubei and Shanghai show signs of deterioration in SSI. The CCI of Sichuan is the lowest at −0.3237. The negative impact of meteorological risks on Guizhou and Yunnan in this study is more severe, which is consistent with the research results of Xue et al. on future drought in Southwest China [2].

### *3.3. The Spatial Evolution of ER*

The level of ER represents the degree to which the YREB is impacted by various economic, social, and ecological factors. The spatial distribution maps of historical and future ER are shown in Figures 5 and 6.

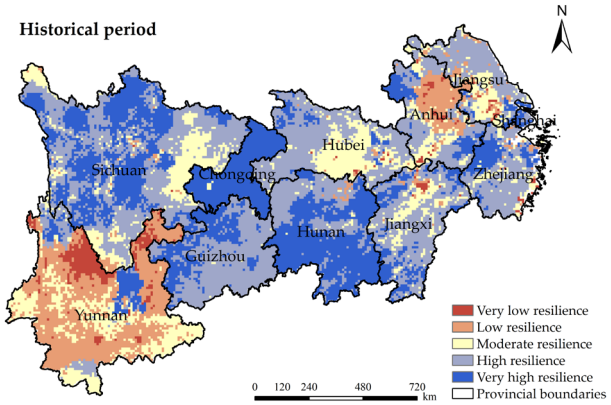


**Figure 5.** Spatial distribution map of ER during historical experimental period.

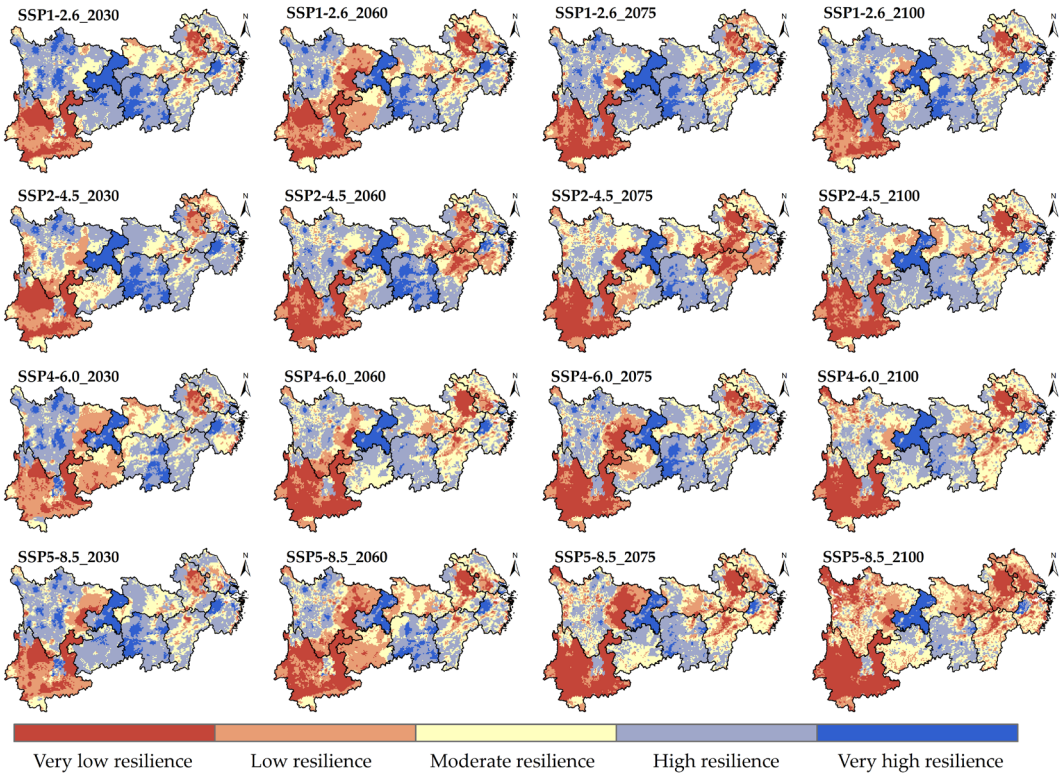


**Figure 6.** Spatial distribution map of ER during future simulation period.

#### 3.3.1. Historical Experimental Period Analysis

From a spatial distribution perspective (Figure 5), the YREB shows an average ER of 0.5259 during the historical period, indicating a moderate resilience level. The mean ER values for the upper, middle, and lower reaches are 0.5298, 0.5239, and 0.5318, respectively, demonstrating a spatial distribution pattern of lower reach > upper reach > middle reach. In particular, areas with very high resilience in the upper reaches are predominantly located in central–western Sichuan, Chongqing, northwestern Guizhou, and central–southern Hunan, with ER values ranging from 0.5423 to 0.6236. The downstream region with very high resilience is located in Shanghai with a toughness value of 0.5806. Notably, high resilience areas are widely distributed and relatively dispersed, mainly around the very high resilience areas centered around Chongqing and Shanghai, while low resilience areas are mainly distributed around moderate resilience areas. Very low resilience areas are located in Yunnan and Anhui, with ER values of 0.4731 and 0.5077, respectively, with the lowest value in Yunnan.

#### 3.3.2. Future Simulation Period Analysis

In comparison to the historical experimental period, the overall level of ER in the future simulation period will decrease (Figure 6). Specifically, in the SSP1-2.6 scenario, the very high resilience zone decreases and high resilience dominates. In 2060, there are large areas of low resilience levels in the upper and lower reaches of the YREB, with values ranging from 0.2840 to 0.5234. The average ER values for the four evaluation years under the SSP2-4.5 scenario are 0.5082, 0.5028, 0.5013, and 0.5017, which are considered moderate resilience levels. Notably, a large range of low and very low resilience areas appeared downstream of YREB in 2075, with ER values ranging from 0.3635 to 0.5023.

The range of moderate and low resilience is further expanded under the SSP4-6.0 scenario. Large areas of moderate and low resilience levels appear in the upstream of 2030, 2060, and 2075, as well as downstream of 2060 and 2100, with resilience values ranging from 0.2854 to 0.5081. Compared to other scenarios, the ER level of the SSP5-8.5 scenario is the lowest, and the range of low and very low resilience areas is expanded. The mean values for the four evaluation years are 0.5096, 0.4893, 0.4887, and 0.4755, respectively. Clearly, there are areas with low resilience levels throughout the entire YREB in 2100, with resilience values ranging from 0.3138 to 0.4362. Notably, Yunnan exhibits the lowest resilience levels in future scenarios in the YREB, while Chongqing maintains the highest resilience levels. Guizhou Province shows the most pronounced decline in ER under future scenarios.

### *3.4. Analysis of Impact of Climate Change on ER*

To quantitatively assess whether the ER under future climate scenarios is significantly influenced by climate change, this study employs the non-parametric Mann–Whitney test to compare the ER levels between four future scenarios and the historical scenario [40]. The results are presented in Table 4.

**Table 4.** Mann–Whitney test.

| | Very Low Resilience | Low Resilience | Moderate Resilience | High Resilience | Very High Resilience | Z | *p* |
|---|---|---|---|---|---|---|---|
| Historical Scenario | 1272 (6.26%) | 2434 (11.98%) | 2662 (13.10%) | 10,003 (49.23%) | 3946 (19.24%) | | |
| SSP1-2.6 | 2378 (11.70%) | 2511 (12.36%) | 4798 (23.62%) | 8421 (41.45%) | 2209 (10.87%) | −34.68 | 0.0011 |
| SSP2-4.5 | 2981 (14.67%) | 3322 (16.35%) | 4989 (24.56%) | 7128 (35.08%) | 1897 (9.34%) | −49.49 | <0.001 |
| SSP4-6.0 | 3042 (14.97%) | 3535 (17.04%) | 5103 (25.12%) | 6969 (34.30%) | 1668 (8.21%) | −53.75 | <0.001 |
| SSP5-8.5 | 3400 (16.73%) | 4238 (20.86%) | 5449 (26.82%) | 5872 (28.90%) | 1358 (6.68%) | −66.15 | <0.001 |

The analysis reveals that the distribution of ER levels in all future scenarios significantly diverges from the historical period ($p < 0.005$), indicating that climate change exerts a profound influence on the spatiotemporal dynamics of ER within the YREB. Based on the absolute values of the test statistic Z, the degree of impact varies significantly across scenarios. The SSP5-8.5 scenario exhibits the largest absolute Z value ($Z = -66.15$), suggesting that its ER distribution deviates most markedly from the historical period and is most severely affected by climate change. This is followed by the SSP4-6.0 and SSP2-4.5 scenarios ($Z = -53.75$ and $Z = -49.49$), while the SSP1-2.6 scenario ($Z = -34.68$) demonstrates a comparatively lower impact.

Further analysis of resilience level proportions indicates that under the SSP5-8.5 scenario, the proportion of very low resilience areas significantly increases from 6.26% in the historical period to 16.73%, while the proportion of very high resilience areas decreases from 19.24% to 6.68%. As shown in the analytical results in Sections 3.1 and 3.2, the SSP5-8.5 scenario exhibits the most pronounced increases in Temp and SSI under intense climate change pressures, along with significant declines in NDVI and SPEI. The combined effects of these multiple meteorological risks result in a significant decrease in ecosystem stability, accompanied by a marked expansion of areas with very low ER. Notably, SSP5-8.5, as the most severe emission pathway in CMIP6, experiences a higher frequency of extreme climate events under this scenario, further exacerbating the pronounced variations in ER levels. In contrast, under the SSP1-2.6 scenario, the proportion of very low resilience areas also increases significantly (from 6.26% to 11.70%), but very high resilience areas persist at a notable level (10.87%). This implies that the adaptive capacity of ecosystems under low-emission pathways remains relatively constrained.

### *3.5. Analysis of CCI Results on ER*

According to the model proposed in Section 2.4, the CCI of ER in 2030, 2060, 2075, and 2100 was calculated for four future scenarios. The CCI heatmap of ER is shown in Figure 7.

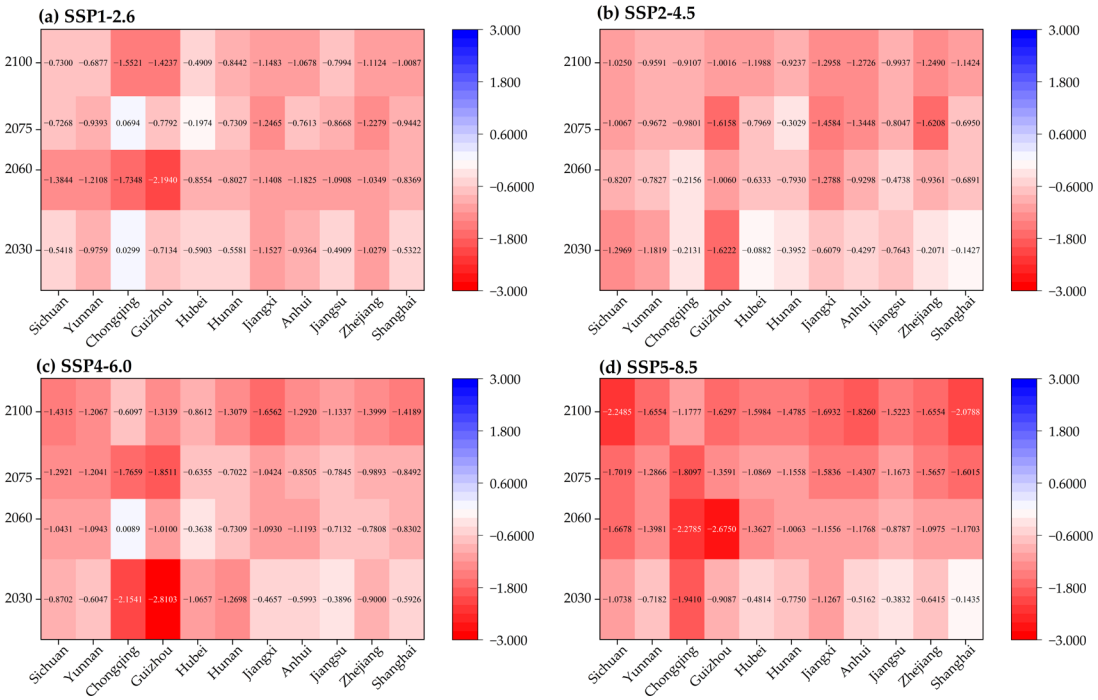


**Figure 7.** CCI heatmap of ER under (**a**) SSP1-2.6 scenario; (**b**) SSP2-4.5 scenario; (**c**) SSP4-6.0 scenario; (**d**) SSP5-8.5 scenario.

3.5.1. Analysis of CCI Results on ER in Temporal Dimension

Under the four future scenarios, the CCI of ER is measured at −0.8005, −0.8924, −0.9540, and −1.2298, respectively, indicating that the ER of the YREB is negatively impacted by climate change. The extent of climate change impacts varies across scenarios, with the ranking SSP5-8.5 > SSP4-6.0 > SSP2-4.5 > SSP1-2.6.

In the SSP1-2.6 scenario (Figure 7a), the overall ER of the YREB is negatively impacted by climate change. The ER of the upper reaches of the YREB (excluding Shanghai) is relatively greatly affected by climate change, with CCI values ranging from −1.1920 to −0.5627. At the same time, the ER of Jiangxi is also greatly affected by climate change, with CCI values of −0.9704, −0.9524, −1.0160, and −1.0732 in the four assessment years. The CCI of Guizhou in 2060 is the lowest under this scenario, at −2.3748. However, the CCI values of Chongqing in 2030 and 2075 are relatively small, at −0.0646 and −0.0792, respectively. This is due to climate change, resulting in a decrease in NDVI and an increase in Temp in the YREB. Elevated temperature can easily cause drought, while accelerated deforestation and urban development can lead to a reduction in forest areas, resulting in a decrease in vegetation coverage.

Compared to the other three scenarios, the ER under the SSP2-4.5 scenario experiences relatively smaller negative impacts from climate change (Figure 7b). Climate change has the greatest negative impact on the ER of Guizhou, with CCI values of −1.2902, −1.3722, −1.3046, and −0.8577 for the four representative years. Secondly, the CCI values of Zhejiang and Jiangxi are relatively large in 2060 and 2075, with values of −1.3673, −1.4367, −1.3819, and −1.4004, respectively. However, the CCI of Shanghai in 2030 is 0.0359, indicating that climate change has an improved impact on its ER. The reason for this trend change is the increase in Temp and decrease in SPEI. The minimum values for Temp and SPEI are 0.6591 and 0.3022, respectively. This means that a decrease in rainfall and high temperatures may lead to drought, which in turn exacerbates the deterioration of ER.

The lower CCI under the SSP4-6.0 scenario is located upstream of the YREB (Figure 7c), indicating that the region suffers more severe negative impacts from climate change. Notably, Guizhou has the lowest CCI in 2030, at −2.3748. The degradation of downstream ER is the most severe in 2100, with CCI values ranging from −1.3015 to −0.8422. In contrast, Chongqing and Shanghai experience relatively weaker negative impacts from climate change, exhibiting CCI values between −0.8853 and −0.1021. Climate change exerts significant influence on the upstream regions, where rising temperatures and declining precipitation collectively increase the risk of drought. Despite the abundance of forest resources in these areas, overexploitation has led to widespread vegetation degradation, which further exacerbates soil erosion.

Compared to the other three scenarios, the ER under the SSP5-8.5 scenario suffers the most severe negative impacts from climate change (Figure 7d), with consistently declining CCI values across the four evaluation years at −0.7015, −1.2910, −1.3124, and −1.6144, respectively. Climate change has a greater negative impact on the upper and lower reaches of the YREB than on the middle reaches. During the four evaluation years, the ER of Sichuan demonstrates relatively severe degradation, with CCI values of −1.0162, −1.6422, −1.7149, and −2.1824, respectively. The CCI of Guizhou in 2060 is −2.3257, which is the minimum value in this scenario. Climate change leads to an increase in Temp and downstream SSI, as well as a decrease in SPEI and NDVI. Due to the relatively developed economy and rapid urbanization process in downstream areas, the proportion of public fiscal expenditure allocated to ecological protection remains inadequate under climate change conditions, which to some extent restricts the effective implementation of ecological restoration projects.

3.5.2. Analysis of CCI Results on ER in Spatial Dimension

Spatially, the upper reaches of the YREB experience stronger negative impacts from climate change on ER, with CCI values ranging from −2.3748 to −0.0646. Future climate change leads to rising temperatures, declining NDVI, and reduced precipitation, collectively causing drought conditions in the region and exacerbating ecological environment degradation. Meanwhile, upstream provinces (e.g., Yunnan, Guizhou) are constrained by insufficient public financial investment, outdated production technologies, and weak environmental awareness, resulting in prominent issues of resource waste and environmental pollution, which significantly weaken the region's ability to respond to meteorological risks. In contrast, Chongqing, as a municipality directly under the central government, has developed strong climate adaptation capabilities due to its advantages in technology and education investment, as well as centralized allocation of financial resources. As a result, it exhibits relatively small negative impacts of climate change, with CCI values ranging from −1.0288 to −0.0646.

The downstream regions of the YREB experience the second most severe negative impacts from climate change after the upstream areas, with CCI values ranging from −1.8834 to −0.0359. The downstream region, which comprises predominantly coastal cities, faces extreme weather events including typhoons, torrential rainfall, and droughts. Particularly, the compounding climate risks formed by the combined effects of sea-level rise and intensified typhoon activity impose additional threats to regional ER and socioeconomic stability. Furthermore, the highly industrialized and densely populated downstream areas exacerbate environmental pollution, leading to increased ecological pressure. Notably, Shanghai demonstrates strong climate adaptation capacity, showing improving trends in ER under both SSP2-4.5 and SSP5-8.5, with CCI values of 0.0359 and 0.0228, respectively. This primarily benefits from its advantageous position as an international trade hub, coupled with strong scientific research capabilities and robust comprehensive economic strength, which collectively enhance its risk response capacity to climate change.

The middle reaches of the YREB experience relatively minor negative impacts from climate change, with CCI values ranging from −1.7496 to −0.1817. The middle reaches feature extensive plains and water networks, with these superior natural resource conditions providing stronger buffering capacity for ecosystems. However, due to the frequent occurrence of extreme weather events such as high temperatures and abnormal precipitation, the ecological environment in this region has suffered certain degradation. At the same time, insufficient investment in environmental protection at the middle reaches has constrained the implementation of ecological restoration projects. Furthermore, poor management of the impacts of climate change may exacerbate environmental pressures, leading to the deterioration of the ecological environment.

## 4. Discussion

(1) Changes in meteorological risks under background of climate change

In this study, compared to the historical period, future scenarios show a rising trend in Temp, while NDVI and SPEI exhibit declining trends. Temp and NDVI are identified as the key drivers leading to the degradation of ER. Notably, changes in temperature, precipitation, and NDVI in Guizhou under future scenarios are particularly pronounced.

Sun, in a study projecting drought and flood disasters in the Yangtze River Basin, showed that the region is expected to experience an overall increase in temperature and a decrease in precipitation in the future [35]. Wen et al. also reached the same conclusion regarding temperature and precipitation in the Yangtze River Basin from 2021 to 2100 [8]. Furthermore, Han et al. found that extreme climate research in Guizhou from 2011 to 2050 showed a prominent decrease in precipitation in the future [38]. Fu et al. used multi-

temporal remote sensing data to analyze long-term vegetation dynamics in the Yangtze River Basin in China and found that the future NDVI showed a trend of prominent decrease upstream and some increase in middle and downstream regions [1]. In conclusion, the findings from the literature are similar to the predicted trends of temperature, precipitation, and NDVI in the future presented in this study.

(2) ER changes in YREB during historical periods

In this study, the ER of the YREB during the historical period was at a moderate level, with an average of 0.5259. The spatial distribution shows downstream (0.5318) > upstream (0.5298) > midstream (0.5239). Specifically, the areas with low resilience upstream are concentrated in Yunnan (0.4731), while the low value areas downstream are mainly distributed in Anhui (0.5077), and the middle reaches are typical in Hubei (0.5223) and Jiangxi (0.5328). It is worth noting that Chongqing (0.6236) and Shanghai (0.5806), as regional cores, exhibit very high resilience values, and ER shows a spatial pattern of decreasing towards the surrounding areas.

Xiao et al.'s study on the YREB from 2010 to 2022 showed that urban resilience follows a distribution pattern of downstream (0.3011) > upstream (0.2010) > midstream (0.1033), with Shanghai, Chongqing, and Zhejiang having the highest mean resilience values, while Jiangxi, Anhui, and Yunnan have lower mean resilience values [41]. This is similar to the spatial distribution of the highest and lowest resilience values in this article. Wang et al.'s research on urban ER in the YREB (2011–2021) shows a distinct east-to-west spatial pattern, eastern regions (Shanghai, Jiangsu, Zhejiang) > central regions (Anhui, Jiangxi, Hubei, Hunan) > western regions (Chongqing, Sichuan, Guizhou, Yunnan), in terms of resilience levels. At the same time, the overall ER of the YREB presents a decreasing trend from central cities such as Shanghai, Nanjing, and Hangzhou to surrounding cities, forming a core–periphery spatial distribution pattern [42]. Lu et al. (2022) also confirmed the gradient pattern of downstream (0.2150) > upstream (0.1053) > midstream (0.0382) in the YREB from 2006 to 2020, and only Shanghai (0.6378) and Chongqing (0.3075) exceeded the regional average, further revealing the spatial distribution structure of core–periphery regions [43], which is highly consistent with the distribution characteristics observed in this study with Chongqing and Shanghai as the center and decreasing towards the periphery.

(3) The spatial differences in river basin ER

In this study, the YREB exhibits spatial differences in ER, characterized by a downstream > upstream > midstream gradient and a concentric pattern of decreasing resilience radiating from the dual cores of Chongqing and Shanghai. Concurrently, the YREB exhibits spatially different responses to climate change, with downstream and upstream regions experiencing more severe negative impacts than midstream areas. Among these regions, Chongqing has developed a high adaptive capacity through prioritized investments in science/technology education and centralized fiscal allocation. Shanghai enhances its risk response capability by leveraging its status as an international hub and its comprehensive economic strength. In contrast, upstream regions such as Yunnan and Guizhou exhibit relatively weaker adaptive capacity due to constraints including insufficient fiscal investment and technological backwardness. The midstream region, while benefiting from natural buffering capacity from its plains and water networks, has suffered ecological degradation due to the increased frequency of extreme climatic events.

This spatial difference pattern has been widely validated across other major river basins. Wang et al. found in their study of urban ER in the Yellow River Basin a distinct core–periphery spatial pattern in the urban agglomeration, characterized by decreasing resilience levels radiating outward from provincial capital cities to peripheral urban areas [44]. Yang et al. further revealed a spatial differentiation pattern in the Yellow River

Basin's urban ER, with higher resilience levels in both upstream and downstream regions compared to the midstream area [24]. Their analysis also showed that upstream resilience is jointly shaped by environmental regulation, industrial structure optimization, technological innovation, and intensive land use; midstream resilience primarily depends on intensive land use, while downstream resilience is mainly influenced by technological innovation and environmental regulation. Wang et al. identified in their study of rural ER in the Jianghan Plain that resilience levels exhibit a distinct southwest–northeast spatial orientation [45]. High resilience zones are primarily influenced by environmental protection spending and population density, while low resilience areas are more strongly influenced by afforestation levels, ecological conservation intensity, and ecosystem stability. Liu et al. noted that the spatial pattern of ER in the Fen River Basin shows a distribution pattern of higher resilience in southern versus northern regions, and elevated levels in eastern/western zones compared to the central area [46]. High resilience zones have superior forest/grass coverage and ecological advantages, while moderate and low resilience zones are more significantly impacted by economic development, population density, and construction land expansion. Although driving factors vary across different river basins, the spatial differences in ER are universally influenced by the combined effects of natural and climatic conditions, socioeconomic investments, and policy regulation.

(4) The changing trend of ER and meteorological risk identification under the background of climate change

This study constructed a quantitative evaluation model coupling climate change and ER based on CMIP6 model data, filling the gap in the integration of climate change and ER research. This model generates the CCI, which is used to quantify the magnitude and directional change in climate impacts on ER. The CCI values for ER under four future climate scenarios are −0.90811, −0.9432, −1.0806, and −1.3812, respectively, indicating that the overall ER of the YREB is declining.

Furthermore, the model can identify meteorological risks. In this study, Temp and NDVI are the main meteorological risks affecting ER. The CCI values for temperature in future scenarios are −0.7630, −0.7884, −0.8229, and −1.0902, respectively, indicating that high temperatures have a deteriorating impact on ER. The CCI values of NDVI are −0.1744, −0.1207, −0.09964, and 0.0587, respectively, which have a deteriorating impact on the YREB as a whole.

## 5. Conclusions

This study develops a coupled quantitative assessment model that integrates climate change and ER based on CMIP6 data for the YREB, which quantifies future climate change impacts on ER through CCI outputs and identifies key meteorological risks affecting ER. The main research results are as follows:

(1) Under the four future scenarios, the CCI values of ER are measured at −0.8005, −0.8924, −0.9540, and −1.2298, respectively, indicating that the ER of the YREB is negatively impacted by climate change. The extent of climate change impacts varies across scenarios, with the ranking SSP5-8.5 > SSP4-6.0 > SSP2-4.5 > SSP1-2.6. The SSP5-8.5 scenario (fossil-fueled development with high radiative forcing) exhibits the most severe impacts, with CCI values of −0.7015, −1.2910, −1.3124, and −1.6144 for the four evaluation years.

(2) Spatially, climate change exerts the greatest impact on the upstream regions, followed by the downstream and midstream areas. Notably, Guizhou Province experiences the most significant ER deterioration, with CCI values of −1.0428, −1.2062, −1.4673, and −1.4204 across the four scenarios.

(3) Temp and NDVI are the primary meteorological risks contributing to the degradation of ER. In future scenarios, Temp shows an increasing trend, with mean values ranging from 0.2627 to 0.4461, while NDVI exhibits a declining trend, ranging from 0.6334 to 0.6825, compared to the historical period. Rising temperatures and reduced precipitation may exacerbate drought conditions, leading to increased soil erosion. Although upstream regions are rich in forest resources, overexploitation and climate-induced vegetation damage pose significant risks. In contrast, downstream regions face intensified ecological pressures due to rapid urbanization and land use changes.

(4) This study still has some limitations, including data inaccuracies and modeling imprecisions. Firstly, the low spatiotemporal resolution of the data inevitably introduces estimation errors. Secondly, the evaluation indicators are limited by data availability, and future studies should incorporate additional ecological metrics to enhance their comprehensiveness. Furthermore, to improve the accuracy of ER estimation and reduce uncertainty, future work could employ multiple models with varied weighting schemes and utilize regional climate model data for more refined analysis. These directions will be explored in subsequent studies.

**Author Contributions:** J.Y. writing—original draft; H.W. writing—revised draft; F.Y. conceptualization, methodology, writing—reviewing and editing. All authors have read and agreed to the published version of the manuscript.

**Funding:** This research was funded by the National Natural Science Foundation of Jiangxi Province, grant number 20243BCE51083; and the Action Plan for Adapting to Climate Change of Jiangxi Province, grant number HX202312110001.

**Institutional Review Board Statement:** Ethical review and approval were waived for this study by Institution Committee due to Legal Regulations (https://www.gov.cn/zhengce/zhengceku/2023-02/28/content_5743658.htm) (accessed on 23 August 2025).

**Informed Consent Statement:** Informed consent for participation was obtained from all subjects involved in the study.

**Data Availability Statement:** All data, models, or code that support the findings of this study are available from the corresponding author upon reasonable request.

**Acknowledgments:** The datasets supporting this study are publicly available from the following sources: (i) The temperature and precipitation observation data: National Meteorological Information Center. Available online: https://data.cma.cn/ (accessed on 12 March 2025). (ii) The CMIP6 global climate model data: ESGF platform. Available online: https://esgf-node.llnl.gov/search/cmip6/ (accessed on 23 April 2025). (iii) NDVI and land use data: Resource and Environmental Science Data Platform. Available online: https://www.resdc.cn/ (accessed on 19 May 2025). (iv) DEM data: Geospatial Data Cloud. Available online: http://www.gscloud.cn/search (accessed on 6 May 2025).

**Conflicts of Interest:** Author Hongliang Wu was employed by the company PowerChina Guizhou Engineering Co., Ltd. The remaining authors declare that the research was conducted in the absence of any commercial or financial relationships that could be construed as a potential confict of interest.

## Abbreviations

The following abbreviations are used in this manuscript:

| | |
|---|---|
| ER | Ecological Resilience |
| YREB | Yangtze River Economic Belt |
| CCI | Climate Change Impact Index |
| Temp | Temperature |
| NDVI | Normalized Difference Vegetation Index |
| AHP | Analytic Hierarchy Process |
| EWM | Entropy Weight Method |

SPEI Standardized Precipitation Evapotranspiration Index
SSI Soil Sensitivity Index

## Appendix A

This study employs a combined EWM-AHP approach to determine the weights of each indicator. The specific calculation method refers to reference [22,23].

### *Appendix A.1. Determining Indices Weights Using AHP*

To ensure the scientific rigor of indicator weighting, we invited three senior experts from the Hydrological Bureau of the Yangtze River Water Resources Commission—Zhou Haoran, Li Xiaohui, and Qian Bao (all with more than 10 years of experience in ecological research in the Yangtze River Basin)—to professionally evaluate the updated indicator system. The selected experts have made significant contributions to their respective fields, such as algal bloom control in the Yangtze River Basin [47], eutrophication of water bodies [48], and phosphorus release processes at the sediment–water interface in lakes in the Yangtze River Basin [49]. Specific methods and calculation formulas can be found in reference [22] (pp. 39–40).

For the convenience of writing, the abbreviations of the 10 indicators are shown in Table A1.

**Table A1.** Abbreviation table of ecological resilience indices.

| **Index Layer** | **Normalized Difference Vegetation Index** | **Annual Temperature** | **Standardized Precipitation Evapotranspiration Index** | **Soil Sensitivity Index** | **The Proportion of Public Financial Expenditure** |
|---|---|---|---|---|---|
| | $Q_1$ | $Q_2$ | $Q_3$ | $Q_4$ | $S_1$ |
| **Index Layer** | **Environmental Protection Expenditure** | **Educational Investment** | **Technology Investment** | **Population Density** | **Proportion of Foreign Direct Investment to GDP** |
| | $S_2$ | $S_3$ | $S_4$ | $S_5$ | $S_6$ |

The three experts rated the selected indicators as shown in Tables A2–A4.

**Table A2.** Expert 1 rating result.

| | **S1** | **S2** | **S3** | **S4** | **S5** | **S6** | **Q1** | **Q2** | **Q3** | **Q4** |
|---|---|---|---|---|---|---|---|---|---|---|
| S1 | 1 | | | | | | | | | |
| S2 | 3 | 1 | | | | | | | | |
| S3 | 2 | 1/2 | 1 | | | | | | | |
| S4 | 3 | 1 | 2 | 1 | | | | | | |
| S5 | 5 | 2 | 4 | 3 | 1 | | | | | |
| S6 | 2 | 1/3 | 1 | 1/2 | 1/4 | 1 | | | | |
| Q1 | 6 | 3 | 4 | 3 | 2 | 4 | 1 | | | |
| Q2 | 7 | 5 | 6 | 5 | 3 | 6 | 2 | 1 | | |
| Q3 | 5 | 3 | 3 | 2 | 1 | 3 | 1/3 | 1/4 | 1 | |
| Q4 | 4 | 2 | 2 | 2 | 0.5 | 3 | 1/4 | 1/5 | 1/3 | 1 |

**Table A3.** Expert 2 rating result.

| | $S_1$ | $S_2$ | $S_3$ | $S_4$ | $S_5$ | $S_6$ | $Q_1$ | $Q_2$ | $Q_3$ | $Q_4$ |
|---|---|---|---|---|---|---|---|---|---|---|
| $S_1$ | 1 | | | | | | | | | |
| $S_2$ | 4 | 1 | | | | | | | | |
| $S_3$ | 3 | 1/4 | 1 | | | | | | | |
| $S_4$ | 5 | 2 | 3 | 1 | | | | | | |
| $S_5$ | 6 | 3 | 4 | 2 | 1 | | | | | |
| $S_6$ | 3 | 1/2 | 1 | 1/3 | 1/3 | 1 | | | | |
| $Q_1$ | 7 | 4 | 5 | 3 | 2 | 5 | 1 | | | |
| $Q_2$ | 8 | 5 | 6 | 4 | 3 | 6 | 3 | 1 | | |
| $Q_3$ | 6 | 3 | 4 | 2 | 1 | 4 | 1/4 | 1/5 | 1 | |
| $Q_4$ | 5 | 3 | 3 | 1 | 1/2 | 3 | 1/5 | 1/6 | 1/2 | 1 |

**Table A4.** Expert 3 rating result.

| | $S_1$ | $S_2$ | $S_3$ | $S_4$ | $S_5$ | $S_6$ | $Q_1$ | $Q_2$ | $Q_3$ | $Q_4$ |
|---|---|---|---|---|---|---|---|---|---|---|
| $S_1$ | 1 | | | | | | | | | |
| $S_2$ | 3 | 1 | | | | | | | | |
| $S_3$ | 2 | 1/2 | 1 | | | | | | | |
| $S_4$ | 4 | 2 | 3 | 1 | | | | | | |
| $S_5$ | 5 | 3 | 5 | 2 | 1 | | | | | |
| $S_6$ | 2 | 1/2 | 1/2 | 1/3 | 1/4 | 1 | | | | |
| $Q_1$ | 6 | 3 | 4 | 2 | 3 | 4 | 1 | | | |
| $Q_2$ | 7 | 4 | 5 | 3 | 2 | 5 | 2 | 1 | | |
| $Q_3$ | 5 | 2 | 3 | 1 | 1/2 | 3 | 1/5 | 1/4 | 1 | |
| $Q_4$ | 4 | 2 | 4 | 1 | 1/3 | 2 | 1/6 | 1/5 | 1/2 | 1 |

To prevent potential data deviation caused by excessive subjectivity in expert questionnaire surveys, we conducted consistency checks for each scoring matrix. The summary results of the consistency check for the three matrices are shown in Table A5.

**Table A5.** Summary of consistency check results.

| | Maximum Eigenvalue | CI | RI | CR | Consistency Check Results |
|---|---|---|---|---|---|
| Expert 1 | 10.401 | 0.045 | 1.49 | 0.0302 | Pass |
| Expert 2 | 10.672 | 0.075 | 1.49 | 0.0504 | Pass |
| Expert 3 | 10.579 | 0.064 | 1.49 | 0.0430 | Pass |

All the matrices listed above have passed the consistency check. The integrated matrix obtained by calculating the geometric mean of three matrices is shown in Table A6.

**Table A6.** An integrated matrix of ecological resilience assessment indices.

| | $S_1$ | $S_2$ | $S_3$ | $S_4$ | $S_5$ | $S_6$ | $Q_1$ | $Q_2$ | $Q_3$ | $Q_4$ |
|---|---|---|---|---|---|---|---|---|---|---|
| $S_1$ | 1.0000 | | | | | | | | | |
| $S_2$ | 3.3019 | 1.0000 | | | | | | | | |
| $S_3$ | 2.2894 | 0.3969 | 1.0000 | | | | | | | |
| $S_4$ | 3.9149 | 1.5874 | 2.6207 | 1.0000 | | | | | | |
| $S_5$ | 5.3133 | 2.6207 | 4.3089 | 2.2894 | 1.0000 | | | | | |
| $S_6$ | 2.2894 | 0.4368 | 0.7937 | 0.3816 | 0.2752 | 1.0000 | | | | |
| $Q_1$ | 6.3164 | 3.3019 | 4.3089 | 2.6207 | 2.2894 | 4.3089 | 1.0000 | | | |
| $Q_2$ | 7.3186 | 4.6416 | 5.6462 | 3.9149 | 2.6207 | 5.6462 | 2.2894 | 1.0000 | | |
| $Q_3$ | 5.3133 | 2.6207 | 3.3019 | 1.5874 | 0.7937 | 3.3019 | 0.2554 | 0.2321 | 1.0000 | |
| $Q_4$ | 4.3089 | 2.2894 | 2.8845 | 1.2599 | 0.4368 | 2.6207 | 0.2027 | 0.1882 | 0.4368 | 1.0000 |

The weights of the integrated matrix were calculated and subjected to consistency testing. The results are shown in Table A7.

**Table A7.** Results of integrated matrix weights and consistency check.

| | Eigenvector | Wight | Maximum Eigenvalue | CI | RI | CR | Consistency Check Results |
|---|---|---|---|---|---|---|---|
| $S_1$ | 0.211 | 2.11% | 10.462 | 0.051 | 1.49 | 0.0342 | Pass |
| $S_2$ | 0.572 | 5.72% | | | | | |
| $S_3$ | 0.353 | 3.53% | | | | | |
| $S_4$ | 0.731 | 7.31% | | | | | |
| $S_5$ | 1.254 | 12.54% | | | | | |
| $S_6$ | 0.345 | 3.45% | | | | | |
| $Q_1$ | 1.986 | 19.86% | | | | | |
| $Q_2$ | 2.769 | 27.69% | | | | | |
| $Q_3$ | 1.033 | 10.33% | | | | | |
| $Q_4$ | 0.748 | 7.48% | | | | | |

*Appendix A.2. Determining Indices Weights Using EWM*

Next, the EWM will be used to calculate the objective weights of each indicator. The basic principles and calculation formulas of the EWM are referenced from reference [23] (pp. 40–41). The calculation results of the Entropy Weight Method are shown in Table A8.

**Table A8.** The result of the EWM.

| Index Layer | Information Entropy | Difference Coefficient | EWM Weight |
|---|---|---|---|
| S1 | 0.9992 | 0.0008 | 0.0312 |
| S2 | 0.9970 | 0.0030 | 0.1226 |
| S3 | 0.9992 | 0.0008 | 0.0345 |
| S4 | 0.9988 | 0.0012 | 0.0496 |
| S5 | 0.9965 | 0.0035 | 0.1456 |
| S6 | 0.9977 | 0.0023 | 0.0925 |
| Q1 | 0.9959 | 0.0041 | 0.1700 |
| Q2 | 0.9953 | 0.0047 | 0.1919 |
| Q3 | 0.9973 | 0.0027 | 0.1102 |
| Q4 | 0.9987 | 0.0013 | 0.0520 |

*Appendix A.3. Comprehensive Determination of Weights Based on EWM-AHP*

The fundamental principle for determining the comprehensive weight is based on reference [23] (p. 42). The comprehensive weight value of the ecological resilience index was ultimately determined, as shown in Table A9.

**Table A9.** ER assessment system for YREB.

| Target Layer | Index Layer | EWM Weight | AHP Weight | Comprehensive Weight |
|---|---|---|---|---|
| ER | Normalized Difference Vegetation Index | 0.4612 | 0.5388 | 0.1783 |
| | Standardized Precipitation Evapotranspiration Index | 0.5163 | 0.4837 | 0.1027 |
| | Annual temperature (°C) | 0.4093 | 0.5907 | 0.2327 |
| | Soil Sensitivity Index | 0.4102 | 0.5898 | 0.0629 |
| | The proportion of public financial expenditure (%) | 0.5969 | 0.4031 | 0.0260 |
| | Technology investment (billion) | 0.4039 | 0.5961 | 0.0612 |
| | Educational investment (billion) | 0.4946 | 0.5054 | 0.0335 |
| | Population density (persons/$km^2$) | 0.5372 | 0.4628 | 0.1310 |
| | Environmental protection expenditure (million dollars) | 0.6820 | 0.3180 | 0.0979 |
| | Proportion of foreign direct investment to GDP (%) | 0.7286 | 0.2714 | 0.0738 |

## References


1. Fu, J.; Liu, J.; Qin, J.; Yang, L.; Zhang, Z.; Deng, Y.; Hu, Y.; Su, B. Monitoring Long-Term Vegetation Dynamics over the Yangtze River Basin, China, Using Multi-Temporal Remote Sensing Data. *Ecosphere* **2024**, *15*, e4809. [CrossRef]
2. Xue, Y.T.; Li, X.H.; Jia, H.J. Future Projection of Drought Risk in Southwestern China Based on CMIP6 Mode. *Res. Soil Water Conserv.* **2023**, *30*, 247–255. [CrossRef]
3. Wang, L.; Zeng, S.D.; Yang, L.H.; Huang, S.S.; Mao, W.Y.; Xia, J. CMIP6-Based Meteorological Drought Characteristic Study under Climate Change in the Hanjiang River Basin. *Water Resour. Prot.* **2024**, *40*, 39–45.
4. Li, H.H.; Sun, S.N. Analysis of the Impact and Response of Climate Change on Extreme Hydrological Events in the Weihe River Basin. *Harnessing Huaihe River* **2024**, *12*, 9–10+21.
5. Liu, K.; Liu, J.F.; Wang, C.Q. Assessment of Future Trends in Temperature and Precipitation in the Yellow River Basin under SSP Scenarios. *J. China Hydrol.* **2024**, *44*, 51–59. [CrossRef]
6. Li, S.X. The Impact of Climate Change on Ecological Security in the Yangtze River Basin. *China Invest.* **2023**, *Z4*, 16–17.
7. Hu, S.S.; Luo, D.; Yang, X.L.; Shi, L.J. Research on Spatio-Temporal Trends of Meteorological Drought in the Yangtze River Basin. *J. China Hydrol.* **2024**, *44*, 76–84. [CrossRef]
8. Wen, S.S.; Wang, Z.C.; Zhai, J.Q.; Jiang, F.S.; Zhou, B. Future Projections of Temperature and Precipitation in Changjiang River Basin Based on N-CMIP6. *Yangtze River* **2024**, *55*, 69–78. [CrossRef]
9. Holling, C.S. Resilience and Stability of Ecological Systems. *Annu. Rev. Ecol. Syst.* **1973**, *4*, 1–23. [CrossRef]
10. Liu, L.; Zhang, Z.; Ding, S.; Yang, F.; Fu, T. Combined Effects of Climate Change on Urban Resilience in the Tibetan Plateau. *Environ. Impact Assess. Rev.* **2023**, *102*, 107186. [CrossRef]
11. Hunt, A.; Watkiss, P. Climate Change Impacts and Adaptation in Cities: A Review of the Literature. *Clim. Change* **2010**, *104*, 13–49. [CrossRef]
12. Cui, Z.; Yang, F.; Ren, F.; Zhang, X.; Jing, Z. Assessing Sustainability Environmental Performance of Three Urban Agglomerations in China: An Input–Output Modeling Approach. *Ecol. Indic.* **2021**, *130*, 108079. [CrossRef]
13. Cannon, T.; Müller-Mahn, D. Vulnerability, Resilience and Development Discourses in Context of Climate Change. *Nat. Hazards* **2010**, *55*, 621–635. [CrossRef]
14. Tompkins, E.L.; Adger, W.N. Does Adaptive Management of Natural Resources Enhance Resilience to Climate Change? *Ecol. Soc.* **2004**, *9*, 10. [CrossRef]
15. Kim, D.; Song, S.-K. Measuring Changes in Urban Functional Capacity for Climate Resilience: Perspectives from Korea. *Futures* **2018**, *102*, 89–103. [CrossRef]
16. Lu, H.; Lu, X.; Jiao, L.; Zhang, Y. Evaluating Urban Agglomeration Resilience to Disaster in the Yangtze Delta City Group in China. *Sustain. Cities Soc.* **2022**, *76*, 103464. [CrossRef]
17. Tang, X.L.; Chen, N. A Multi-Scenario Urban Resilience Simulation Study Based on the System Dynamics Model. *Phys. Chem. Earth Parts A/B/C* **2023**, *132*, 103467. [CrossRef]
18. Xia, C.H.; Zhai, G.F. The Spatiotemporal Evolution Pattern of Urban Resilience in the Yangtze River Delta Urban Agglomeration Based on TOPSIS-PSO-ELM. *Sustain. Cities Soc.* **2022**, *87*, 104223. [CrossRef]
19. Liu, L.N.; Lei, Y.L.; Zhuang, M.H.; Ding, S. The Impact of Climate Change on Urban Resilience in the Beijing-Tianjin-Hebei Region. *Sci. Total Environ.* **2022**, *827*, 154157. [CrossRef]
20. Chang, Q.; Sha, Y.; Chen, Y. The Coupling Coordination and Influencing Factors of Urbanization and Ecological Resilience in the Yangtze River Delta Urban Agglomeration, China. *Land* **2024**, *13*, 111. [CrossRef]
21. Chen, H.B. Collaborative Promotion of Ecological Priority and Green Development in the Yangtze River Economic Belt: From the Perspective of Biodiversity. *Stud. Social. Chin. Charact.* **2020**, *3*, 79–87.
22. Chen, Y. Research on Risk Management of Real Estate Trustee-Construction Based on the Analytic Hierarchy Process-a Case Study of the BGY-TH Project. *Jilin Univ.* **2024**, *8*, 1–75.
23. Han, M. Customer Value Analysis and Marketing Strategy Research of R Company Based on AHP-Entroph Method. *Beijing Univ. Chem. Technol.* **2019**, *6*, 1–77.
24. Yang, L.S.; Chen, Y.; Xie, H.Q. Spatio-Temporal Patterns and Driving Factors of Ecological Resilience in Urban Agglomerations in the Yellow River Basin. *Ecol. Econ.* **2024**, *40*, 99–108.
25. Ye, C.; Hu, M.; Lu, L.; Dong, Q.; Gu, M. Spatio-Temporal Evolution and Factor Explanatory Power Analysis of Urban Resilience in the Yangtze River Economic Belt. *Geogr. Sustain.* **2022**, *3*, 299–311. [CrossRef]
26. Wu, Z.Y.; Sun, S.; Zhang, S.Y.; Wang, W. Climate Resilience Assessment and Enhancement Countermeasures for Yellow River Basin Cities. *Sci. Technol. Manag. Land Resour.* **2021**, *41*, 62–74.
27. Lu, F.; Liu, Q.; Wang, P. Spatiotemporal Characteristics of Ecological Resilience and Its Influencing Factors in the Yellow River Basin of China. *Sci. Rep.* **2024**, *14*, 16988. [CrossRef]
28. Zhong, P.S. Comparative Study on Ecological Resilience between the Yangtze River Economic Belt and the Yellow River Basin. *Xinyang Norm. Univ.* **2024**, *4*, 1–88. [CrossRef]

29. Tao, J.Y.; Dong, P.; Lu, Y.Q. Analysis of Spatiotemporal Changes and Influencing Factors of Ecological Resilience in the Yangtze River Delta Region. *Resour. Environ. Yangtze Basin* **2022**, *31*, 1975–1987.
30. Lu, L. Analysis on Spatial-Temporal Characteristics and Its Influencing Factors of Urban Resilience in the Yangtze River Economic Belt. *East China Univ. Technol.* **2021**, *3*, 1–86.
31. Zhou, C.; Zhao, Y.L.; Zhang, X.H.; Zhou, L.; Ren, M.M. Spatiotemporal Evolutionary Characteristics and Coordinated Development of Urban Ecological Resilience and Efficiency in the Yellow River Basin. *Arid. Land Geogr.* **2022**, *46*, 1514–1523.
32. Swain, S.S. Assessment of Basin-Scale Concurrent Dry and Wet Extreme Dynamics under Multimodel CORDEX Climate Scenarios. *Int. J. Climatol.* **2024**, *44*, 5950–5968. [CrossRef]
33. Wei, J.M.; Li, C.B.; Wu, L.; Xie, X.H.; Lv, J.N.; Zhou, X. Study on Soil Erosion in Northwestern Sichuan and Southern Gansu (NSSG) Based on USLE. *J. Soil Water Conserv.* **2021**, *35*, 31–37+46. [CrossRef]
34. Wang, Z.Y. Research on Risk Assessment of Soil and Water Loss in Jiangsu Province by Coupling RUSLE Model and Multi-Source Data. *Shaanxi Water Resour.* **2023**, *10*, 107–109. [CrossRef]
35. Sun, F.Y. Drought and Flood Outlook for the Yangtze River Basin. *East China Norm. Univ.* **2018**, *5*, 1–187.
36. Wei, J.; Wang, Z.; Han, L.; Shang, J.; Zhao, B. Analysis of Spatio-Temporal Evolution Characteristics of Drought and Its Driving Factors in Yangtze River Basin Based on SPEI. *Atmosphere* **2022**, *13*, 1986. [CrossRef]
37. Gong, X.; Du, S.; Li, F.; Ding, Y. Study of Mesoscale NDVI Prediction Models in Arid and Semiarid Regions of China under Changing Environments. *Ecol. Indic.* **2021**, *131*, 108198. [CrossRef]
38. Han, H.Q.; Zhang, J.Y.; Su, Z.H.; Lu, Y. Spatial and Temporal Variations of Extreme Climate Indices in Guizhou Province from 2011 to 2050. *Res. Soil Water Conserv.* **2018**, *25*, 341–346. [CrossRef]
39. Li, X.N.; He, L.H.; Xue, L.Q. Spatial-Temporal Differentiation and Prediction of Extreme Weather Events and Vegetation Cover in Guizhou Province under Climate Change. *Pearl River* **2024**, *45*, 65–75.
40. Wang, R.L.; Pan, W.L.; Wang, X.Q. Non-Parametric Two-Sample Test Developments and Prospects. *Chin. J. Appl. Probab. Stat.* **2024**, *40*, 498–524. [CrossRef]
41. Xiao, Y.; He, L.; Li, M.K.; Yu, Y.; Meng, J.Y.; Zhou, Y. Dynamic Evolution and Regional, Variance of Urban Resilience in Yangtze River Economic Zone. *Resour. Ind.* **2025**, *7*, 1–13. [CrossRef]
42. Wang, Z.F.; Liang, Z.Q. Evolution Pattern and Prediction of Ecological Resilience of Cities in the Yangtze River Economic Belt. *Resour. Environ. Yangtze Basin* **2025**, *34*, 268–279.
43. Lu, F.Y.; Zhang, C.; Jia, T.Y.; Huang, Z.F.; Xu, M. Spatio-Temporal Evolution Characteristics and Driving Mechanisms of Urban Ecological Resilience in the Yangtze River Economic Belt. *Environ. Sci.* **2025**, *46*, 4592–4601. [CrossRef]
44. Wang, S.M.; Niu, J.L. Spatio-Temporal Evolution and Influencing Factors of Urban Ecological Resilience in the Yellow River Basin. *Acta Ecol. Sin.* **2023**, *43*, 8309–8320. [CrossRef]
45. Wang, D.; Jiao, Y.; Jiao, W.X.; Wang, H.; Zheng, H.R. Spatio-Temporal Evolution and Driving Factors of Rural Ecological Resilience in Jianghan Plain. *J. Cent. China Norm. Univ. (Nat. Sci.)* **2024**, *58*, 255–263. [CrossRef]
46. Liu, H.L.; Wang, G.Y.; Zhang, P.C.; Wang, Z.L.; Zhang, L.P. Spatio-Temporal Evolution and Coordination Influence of Coupling Coordination between New Urbanization and Ecological Resilience in Fenhe River Basin. *J. Nat. Resour.* **2024**, *39*, 640–667. [CrossRef]
47. Chen, F.; Wang, W.J.; He, T.; Zhou, H.R.; Qian, B. Analysis on Status and Countermeasures for Bloom Growth in Middle and Lower Hanjiang River. *Yangtze River* **2023**, *54*, 7–17. [CrossRef]
48. Chen, F.; Li, X.H.; Wang, W.J.; Peng, L.; Qian, B. Temporal and Spatial Variation Characteristics of Total Phosphorusin Yangtze River Basin from 2018 to 2022. *Express Water Resour. Hydropower Inf.* **2023**, *44*, 91–97. [CrossRef]
49. Qian, B.; Liu, L.; Xiao, X.; Chen, M.S. The Process of Phosphorus Release from Lake Sediments on the Micro-Interface. *J. Hydraul. Eng.* **2014**, *45*, 482–489. [CrossRef]


**Disclaimer/Publisher's Note:** The statements, opinions and data contained in all publications are solely those of the individual author(s) and contributor(s) and not of MDPI and/or the editor(s). MDPI and/or the editor(s) disclaim responsibility for any injury to people or property resulting from any ideas, methods, instructions or products referred to in the content.